

# Multimode Jahn-Teller Effect in Negatively Charged Nitrogen-Vacancy Center in Diamond

Jianhua Zhang,<sup>1,2</sup> Jun Liu,<sup>2</sup> Z. Z. Zhu,<sup>3</sup> K. M. Ho,<sup>2</sup> V. V. Dobrovitski,<sup>4</sup> and C. Z. Wang<sup>2</sup>

<sup>1</sup>*School of Physics and Optoelectronic Engineering, Hainan University, Haikou, 570228, China*

<sup>2</sup>*Ames Laboratory-U.S. DOE and Department of Physics and Astronomy, Iowa State University, Ames IA 50011, USA*

<sup>3</sup>*Collaborative Innovation Center for Optoelectronic Semiconductors and Efficient Devices,*

*Department of Physics, Xiamen University, Xiamen 361005, China*

<sup>4</sup>*QuTech and Kavli Institute of Nanoscience, TU Delft, P.O. Box 5046, 2600 GA Delft, Netherlands*

Multimode Jahn-Teller (JT) effect in a negatively charged nitrogen-vacancy (NV) center in its excited state is studied by first-principles calculations based on density function theory (DFT). The activation pathways of the JT distortions are analyzed to elucidate and quantify the contribution of different vibrational modes. The results show that the dominant vibrational modes in the JT distortions are closely related to the phonon sideband observed in two-dimensional electronic spectroscopy (2DES), consistent with *ab initio* molecular dynamics (AIMD) simulation results. Our calculations provide a new way to understand the origin and the mechanism of the vibronic coupling of the system. The obtained dominant vibrational modes coupled to the NV centre and their interactions with electronic states provides new insights into dephasing, relaxation and optically driven quantum effects, and are critical for the application to quantum information, magnetometry and sensing.

The negatively charged nitrogen-vacancy (NV) center in diamond has attracted significant attention for its potential applications in various technologies[1, 2], including quantum information[3, 4], magnetometry[5, 6], and photonics[7, 8]. The center also present an excellent platform for studying fundamental quantum mechanics problems such as the dynamics of quantum spins coupled to their environment[9, 10], and exploring quantum control of solid-state spins[11, 12].

Lattice vibrations play a crucial role in many properties of the NV center. Vibrational modes participate in the optical transition and are responsible for the visible sideband in the absorption or photoluminescence spectra[13]. Phonons also strongly influence on the relaxation of electronic orbitals[14], the decoherence of spin states[15], and the depolarization of the emitted photons[16]. Particularly, electron-phonon coupling induces JT distortion in the  ${}^3E$  excited state of the NV center, significantly impacting the dynamics of the state[16, 17]. Besides, the dynamical JT effect (dJTe) is demonstrated to be the dominant dephasing mechanism for optical transitions[16], and the electronic depolarization dynamics[18] of the NV center.

Theoretical modeling using multiphonon model[19] and accurate first principles calculations[20, 21] were carried out to reproduce the vibronic band and successfully describe the luminescence and adsorption lineshapes of the NV center. Other *ab initio* calculations examined the localized or quasilocated vibrational modes[22, 23], confirmed the existing dJTe in the excited state of the NV center[17], and suggested that the dJTe is responsible for the multiple intersystem crossing rates at cryogenic temperatures[24].

Previous *ab initio* calculations for the dJTe of the NV center in the excited state assumed it to be an ideal  $E \otimes e$  JT system, considering only a doubly degenerate  $e$  vibrational mode in the JT distortion process[17, 24]. However, it is known that for a JT center system with  $N$  atoms, there are  $3N - 3$  degrees of freedom, conveniently described by normal vibration coordinates with corresponding irreducible representations of the symmetry point group of the JT center in the harmonic approximation. If  $N$  is not small, there may be more than one active mode participating in the JT distortion process, known

as the 'multimode JT problem'[25]. These active modes may have different nature and distinct roles in the dynamics. It's reasonable to infer that the active modes directly impact the center's dynamics, thereby influencing its electronic, spin, and optical properties. Thus, understanding the multimode JT problem, especially the dynamical path of JT distortion, is crucial and requires more careful study. Recently, based on a finite supercell mode, we used an intrinsic distortion path (IDP) method to investigate the multimode JT problem in the ground state of the neutral NV center[26]. The main idea of the IDP method is to express the JT active distortion as a linear combination of normal modes in the low symmetry (LS) energy minimum geometry. Using this approach, one can identify the vibrational modes which have a large contribution to the JT distortion. In this work, we use a combination of DFT calculations and the IDP method to investigate the effects of multimode JT distortion in the NV center in diamond. We find that several vibrational modes have large contributions to the JT distortion. These identified vibrational modes are strongly associated with the strongly coupled vibrational modes to the NV center observed through two-dimensional electronic spectroscopy (2DES) measurements[27, 28].

The NV center exhibits  $C_{3v}$  symmetry in its  ${}^3A_2$  ground state. Its electronic structure defect state comprises two fully symmetric singlet  $A_1$  states ( $u\bar{u}v\bar{v}$ ) and one doubly degenerate  $E$  state ( $e_x\bar{e}_xe_y\bar{e}_y$ ), with six electrons occupying  $u^2v^2e^2$  in the ground state[29]. The  ${}^3E$  excited state is achieved by promoting an electron from a singlet  $\bar{v}$ (or  $v$ ) to the doublet  $\bar{e}_x$  or  $\bar{e}_y$  state, resulting in a  $u^2v^1e^3$  configuration (Fig. 1). In this configuration, the degenerate  $E$  state is only partially occupied, leading to instability due to the JT effect. Consequently, the system tends to distort into a more stable nondegenerate geometry with lower ( $C_{1h}$ ) symmetry.

The DFT calculations utilized the projector augmented wave (PAW) method with spin polarization, implemented in VASP[30]. Hybrid density (HSE06)[31] functional were employed as the exchange-correlation functionals in the geometry optimization and adiabatic potential energy surface (APES) calculations. A kinetic energy cutoff of 400 eV (HSE06) for the plane wave basis set and the  $\Gamma$  point for  $k$ -

TABLE I. Ab initio parameters of APES.  $\rho_{JT}^M$  ( $\rho_{JT}^S$ ) represents the distance of the vector from a minimum state (saddle point) to the high symmetry ( $C_{3v}$ ) state.  $E_{JT}^M (= E_{HS}^M - E_{LS}^M)$  and  $E_{JT}^S (= E_{HS}^S - E_{LS}^S)$  denote the energies of a minimum and a saddle point with respect to the high symmetry state.  $\Delta$  is the barrier energy between  $G_M$  and  $G_S$ .

	$\rho_{JT}^M(\text{\AA})$	$E_{JT}^M(\text{meV})$	$\rho_{JT}^S(\text{\AA})$	$E_{JT}^S(\text{meV})$	$\Delta(\text{meV})$
HSE06	0.0699	41.0	0.0753	38.5	9.9

point sampling were employed. A 216-atom ( $3 \times 3 \times 3$ ) cubic supercells with the box length of  $3a_0 = 10.632\text{\AA}$  (HSE06) were used, where  $a_0$  is the diamond lattice constant optimized by DFT calculation. A standard fraction of screened Fock exchange  $\mu = 0.2$  and the default value of mixing parameter  $a = 0.25$  were utilized in the HSE06 calculations[31]. A high-symmetry (HS)  $C_{3v}$  configuration of the NV center in the excited state is obtained by the geometry optimization with an average electronic occupation in each of the  $\bar{e}$  orbitals,  $(\bar{e}_x)^{0.5}(\bar{e}_y)^{0.5}$  (Fig. 1, middle). Using this optimized configuration, the energies  $E_{HS}^M$  and  $E_{HS}^S$  of the NV center with an integer occupation  $(\bar{e}_x)^1(\bar{e}_y)^0$  for the lower branch and  $(\bar{e}_x)^0(\bar{e}_y)^1$  for the upper branch of the excited state respectively are calculated. These two energies have a small difference due to the origin of DFT calculations[32, 33]. Then, geometry optimization proceeds with  $C_{1h}$  symmetry constraints, resulting in low symmetry (LS)  $C_{1h}$  structures. The APES of the yielding different LS  $C_{1h}$  structures contains geometries: three energy minima ( $G_M$ ) with electronic occupation  $(\bar{a}'')^1(\bar{a}')^0$  and three saddle points ( $G_S$ ) with electronic occupation  $(\bar{a}')^1(\bar{a}'')^0$  as shown in Fig. 2(b). The energies  $E_{LS}^M$  for  $G_M$  and  $E_{LS}^S$  for  $G_S$  are calculated. By varying the coordinates of ions, the energy of other points in APES can be obtained. In the high symmetry geometry ( $G_{HS}$ ) (Fig. 1: middle) the three C atoms adjacent to the vacancy site are equivalent, forming an equilateral triangle. For  $G_M$  and  $G_S$  in the LS structure, the atomic bond between two of the three C atoms ( $C_2$  and  $C_3$ ) near the vacancy is elongated (Fig. 1: right) or compressed (Fig. 1: left) resulting in inducing two low-symmetry isosceles triangles. The calculated JT parameters can be found in Table I.

To analyze the electron-phonon coupling in the APES obtained by the total energy calculation, the electronic Hamiltonian  $H$  of the system can be expanded as a Taylor series around  $G_{HS}$  with respect to the  $3N - 3$  normal vibration coordinates  $Q_{HSk}$ . The corresponding matrix element can be written as [33]  $H_{ij} = E_0\delta_{ij} + \sum_{k=1}^{3N-3} \sum_{i,j}^f F_{ij}^k Q_{HSk} + 1/2 \sum_{k=1}^{3N-3} \sum_{i=1}^f G_{ii}^{kk} Q_{HSk}^2 + 1/2 \sum_{k,l=1; k \neq l}^{3N-3} \sum_{i,j=1; i \neq j}^f G_{ij}^{kl} Q_{HSk} Q_{HSl} + \dots$ , (1) where  $E_0$  is the energy of electronic Hamilton of the  $G_{HS}$ ,  $F_{ij}^k$ ,  $G_{ii}^{kk}$ ,  $G_{ij}^{kl}$  are the vibronic coupling constants, and the index  $f$  reminds that the ground state eigenfunction of  $H$  is  $f$ -fold degenerate. The distortion from an HS geometry, caused by the JT effect, towards a LS geometry corresponding to one of the energy minima is a displacement on the  $3N - 3$  potential energy surface. This distortion usually involves multiple vi-

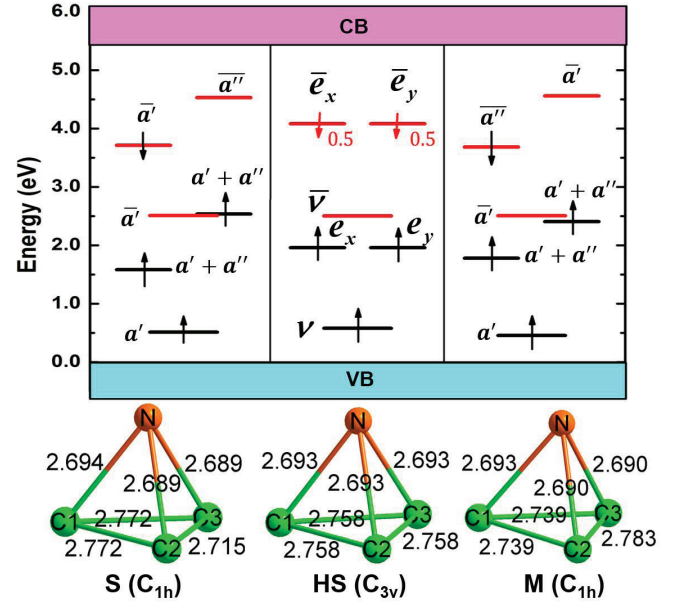


FIG. 1. (Color online) Structure (lower panel) and relevant single-electron orbitals (upper panel) of negatively charged NV-center in the excited state: the saddle point (S, left), the  $C_{3v}$  high symmetry state (HS, middle), the distorted  $C_{1h}$  minimum state (MIN, right). As the geometry distorts from HS to M (or S), the degeneracy of electronic configuration  $(\bar{e}_x)^{0.5}(\bar{e}_y)^{0.5}$ , resulting in a new configuration:  $(\bar{a}'')^1(\bar{a}')^0$  for M and  $(\bar{a}')^1(\bar{a}'')^0$  for S. In the lower panel, only first neighbor C (green sphere) and N (yellow sphere) atoms to the vacant site are shown. The distances in  $\text{\AA}$  between the first neighbor atoms are also shown. In the upper panel, only the states between the valence band (VB) and conduction band (CB) are shown. The energies are given with respect to the top of the VB. The symbols with the bar denote the spin-down states, the symbols without the bar correspond to the spin-up states. The states  $\nu$  and  $\bar{\nu}$  have  $a_1$  symmetry, all other states have  $e$  symmetry.

brational modes, but sometimes it can be simplified to a single effective mode[25]. The NV center in the excited state with the  $C_{3v}$  point group symmetry exhibits a two-fold degeneracy  $E$  state which can cause a  $E \otimes e = a_1 + [a_2] + e$  splitting. Only the asymmetric displacement  $e$  can distort the system from the HS  $C_{3v}$  configuration toward to the LS  $C_{1h}$  structure. In general, the degenerate electronic states of a JT system undergo distortion to a lower symmetry configuration along the degenerate vibrational modes. As a result, the electronic degeneracy is lifted and two separate APES sheets with a conical intersection are formed. The JT effect splits the doubly degenerate  ${}^3E$  state into two sheets of energy surfaces with the lower sheet exhibiting a tricorner structure (Fig. 2), consistent with the standard  $E \otimes e$  picture. Our calculations also suggest that support the dJTe arising from the excited  ${}^3E$  state of the NV center. The adiabatic potential minima are shallow ( $E_{JT}^M = 41 \text{ meV}$ ), and the distorted LS configurations are difficult to observe at room temperature[25]. The results at the HSE06 level are in a good agreement with the standard  $E \otimes e$  picture, showing small energy barriers between minima ( $\Delta = 9.9 \text{ meV}$ ) and enabling near-free pseudorotation at ambient temperature.

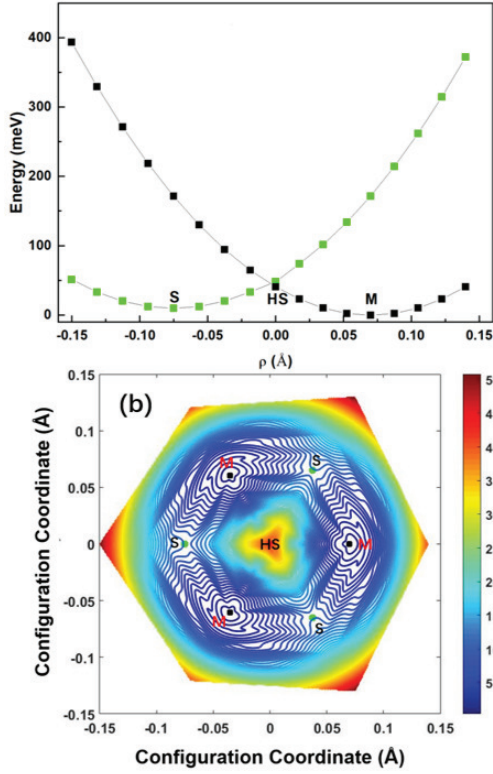


FIG. 2. (Color online) Adiabatic potential energy surface (APES) of the negatively charged NV-center along  $\rho_{JT}^M$  (positive) and  $\rho_{JT}^S$  (negative) directions in the excited states via DFT calculations. All the points (red points) shown in the figure are ab initio energies calculated from HSE06. The black solid lines are the quadratic fit of the ab initio energies based on Eq. (2). The energy shown in the vertical axis is with respect to the energy minimum point (M). (b) Contour plot of the lower sheet of the  $^3E$  excited states on APES in the surface formed by  $\rho_{JT}^M$  and  $\rho_{JT}^S$ . The position of minima M (black points) and saddle points S (green points) are also shown. The high symmetry point corresponding to the  $G_{HS}$  is at the center. The energy (in unit meV) shown in the figure is with respect to the energy of the  $G_M$ .

To further analyze the multimode JT problem of the NV center, we employ the IDP method with the LS configuration as the reference point. The IDP method[33, 34] relies on the fact that all information needed for description of the vibronic coupling is contained in the distorted LS minimum energy geometry  $G_M$ . Therefore, one can choose the  $G_M$  as a reference and the distortion can be expressed as the superposition of all normal modes in the quadratic well at the  $G_M$ . Within the harmonic approximation, the energy of a point X on the APES around an energy minimum can be represented using a quadratic energy surface[33, 34]:  $E_X = \sum_{k=1}^{N_{a1}} E_k = 1/2 \sum_{k=1}^{N_{a1}} w_{Xk} v_k \vec{Q}_k \cdot \vec{Q}_k$ , (3) where  $\vec{Q}_k$  and  $v_k$  are the eigenvectors and frequencies of the vibrational modes in  $G_M$ .  $w_{Xk}$  are weighing factors and  $N_{a1}$  is the number of all totally symmetric normal modes. The vibrational modes used here are calculated using a finite-displacement method by first-principles calculations only at the PBE level[35], because HSE calculations are up to two orders of magnitude

more expensive than PBE calculations and the relevant vibrational modes, are very similar in both cases[20]. The system is driven along a path from the point X to the energy minimum point step by step by according to the driving forces[33, 34]:  $\vec{F}_{Xtot} = \sum_{k=1}^{N_{a1}} \vec{F}_{Xk} = 1/2 \sum_{k=1}^{N_{a1}} w_{Xk} v_k M^{1/2} \vec{Q}_k$ , (4) where  $\vec{F}_{Xk}$  is the forces induced by different normal modes which are obtained from the derivative of energy over the Cartesian coordinates of the normal modes, and  $M$  is a diagonal  $3N \times 3N$  matrix containing the atomic masses in triplicates as elements  $(m_1, m_2, m_3, m_4, \dots, m_n)$ [34]. This path driven by the forces in Eq. (4) is called the intrinsic distortion path (IDP). The distortion vector  $\vec{R}_x$  (from the point X to the energy minimum point M) can be expressed in terms of the normal modes in  $G_M$ [33, 34],  $\vec{R}_x = \sum_{k=1}^{N_{a1}} w_{Xk} \vec{Q}_k$ . (5)

Particularly if X is exactly on the HS unstable point in the cusp of the lower sheet of APES, the distortion  $vecR_x$  becomes the JT distortion  $\vec{R}_{JT}$ , while the corresponding energy is JT energy ( $E_{JT}$ ). The IDP analysis gives a further insight into the vibronic coupling in NV center. The potential energy profile along the IDP for the distortion from the cusp to the global minimum presented in Fig. 3(a) delineates two different regions. In the first region, the energy changes fast, and most of the  $E_{JT}$  is gained after 40% of the path is covered. In the second region, the system has just relaxed towards the global minimum. The IDP is slightly different from the direct path (DP), which is defined by the straight path along the vector  $R_{JT}^M$  in the APES. The energies along DP were calculated in the interaction mode way using equations (3) and (5). The IDP is steeper than the DP, and the system is strongly and quickly stabilized along the path (Fig. 3(a)). The energies calculated via DFT along the IDP and DP agree well with those within harmonic approximation, but a small deviation arises as they approach  $G_{HS}$ . Especially the JT energy (37.7 meV) obtained from the IDP method is lower than that ( $E_{JT}^M = 41.0$  meV) obtained from DFT calculation. The differences of the IDP method and DFT calculations would be partially attributed to the anharmonicity of the NV system[34, 36]. The energy barrier  $\Delta$  (about 29.8 meV) between two neighboring minima obtained by IDP method within the harmonic approximation is higher than the one ( $\Delta = 9.9$  meV) obtained by DFT calculation (Fig.3(b)). This discrepancy arises because the harmonic approximation employed in the IDP method neglects anharmonic effects, which substantially soften the adiabatic potential energy surface. In contrast, the fully self-consistent DFT calculations capture these effects, leading to a markedly reduced energy barrier associated with the Jahn–Teller distortion.

Within the harmonic approximation, it is possible to quantify the contributions of different normal modes to the JT distortion and their changes along the IDP. Specifically, in  $G_M$  several totally symmetric  $a1$  modes (45.0 meV, 57.8 meV, and 64.0 meV) have main contributions to the lattice distortion from  $G_M$  to  $G_{HS}$ , accounting for approximately 31.1%, 29.8%, and 9.1%(Fig. 3c), respectively. While the dominant modes (31.6 meV, 46.5 meV, 57.3 meV) in the JT distortion from  $G_S$  to  $G_M$  contribute 43.6%, 17.0%, and 8.6% to the distortion(Fig. 3d), respectively. The contribu-

TABLE II. Analysis of the multimode JT effect in the excited state of NV center. Modes I (II) are the vibrational modes with large contributions to the JT distortion from the high symmetry geometry (the saddle point) to the energy minimum.  $c_{r,m}^k$  and  $c_{e,s}^k$  are the contributions of the chosen normal modes to the distortions  $R_M$  and  $R_S$ .  $c_{e,m}^k$  and  $c_{e,s}^k$  are the contributions of the normal modes to the energies  $E_M$  and  $E_S$ . The numbers in parentheses in the second and fifth columns represent the count of vibration modes with close frequencies. The results from the 2DES experiment([27] / [28]) and the AIMD calculation at 10K/77K [18] are also shown in the table for comparison.

Modes I (meV)	$c_{r,m}^k$ (%)	$c_{e,m}^k$ (%)	Modes II (meV)	$c_{r,s}^k$ (%)	$c_{e,s}^k$	2DES (meV)	AIMD (meV)
			31.6	43.6(1)	11.0	32.1±2.4 / 36.3	35.7 / 32.0
45.0±0.8	31.1(3)	11.7	46.5±1.8	17.0(5)	9.5	41.8±3.8 / 47.5	46.8 / 46.9
57.8±2.4	29.8(5)	15.0	57.3±2.0	8.6(9)	6.7	56.7±2.2	55.2 / 57.7
64.0±0.5	9.1(4)	7.0	63.4±1.9	6.3(6)	6.3		
66.1±0.5	1.2(2)	1.0	66.3±0.3	1.9(2)	2.1	69.2±2.0 / 66.2	66.2 / 68.6
75.3±1.3	3.9(5)	4.1	75.9±0.7	2.2(3)	3.3	/ 75.0	/ 76.8
81.8±0.8	4.8(5)	5.4	81.4±1.1	1.8(5)	3.1	79.8±2.6	79.9 /
86.5±0.7	2.4(2)	2.9	86.8±1.5	1.9(5)	3.7	/ 85.3	88.1 / 88.1
94.9±0.9	1.7(4)		95.3±0.1	1.0(2)	2.3	91.3±2.2	93.6 / 93.3
106.5±0.1	0.6(2)	1.3				105.7	110.2 / 107.2
			127.9	0.3(1)	1.1	127.5±2.7	126.7 / 126.8
147.9	0.3(1)					144.6±2.7	146.0 / 148.5
157.3	0.4(1)	1.9	156.9	0.6(1)	3.6	156.5	154.4 / 156.7
164.5	1.6(1)	8.1	164.0±0.9	1.5(2)	9.9	166.0±2.7	159.8 / 162.4
Total	87.0	64.7		87.9	62.5		

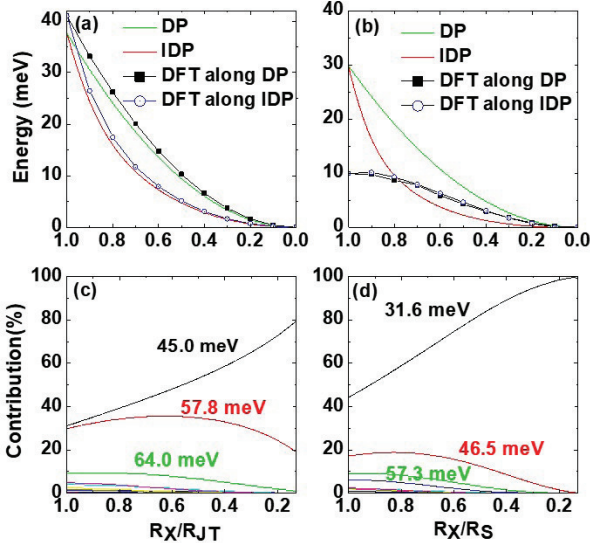


FIG. 3. (Color online) (a, b) Energy changes from (a) the  $G_{HS}$  ( $R_X/R_{JT} = 1$ ) and (b) the  $G_S$  ( $R_X/R_S = 1$ ) to the  $G_M$  ( $R_X/R_{JT} = 0$ ) along the direct path and IDP. (c, d) The contributions (normalized to 1) to the distortion from the most important normal modes along the IDP from (c) the  $G_{HS}$  ( $R_X/R_{JT} = 1$ ) and (d) the  $G_S$  ( $R_X/R_S = 1$ ) to the  $G_M$  ( $R_X/R_{JT} = 0$ ).

tions vary along the IDP [Fig. 3(c, d)], indicating the importance of each mode in the JT distortion depends on the distance away from  $G_{HS}$  (or  $G_S$ ). Interestingly, the contributions of the most significant modes (45.0 meV in Fig. 3(c) and 31.62 meV in Fig. 3(d)) increase while the contributions of the other modes decrease along the distortion. There are 36 (and 42) vibrational modes are displayed in the Table II for their significant contributions (exceeding 0.25%) to the JT distortion from  $G_{HS}$  (or correspondingly  $G_S$ ) to

$G_M$ . Their total contributions to the distortions are about 87.0% and 87.9%, while they contribute 64.7% to the JT energy and 62.5% to the energy barrier between two minima. Most of the JT-active modes found in the IDP method have been observed in the vibrational bath in the 2DES experiment[27]. Two modes (22.6 meV and 189.1 meV) in the vibrational bath are probably associated with delocalized diamond lattice dynamics[27] and are not found in the JT distortion. Two vibrational modes at 106.5 meV and 157.3 meV/156.9 meV closely match those observed in 2DES experiments (105.7 meV and 156.5 meV), as evidenced by prominent peaks in their FFT spectra (Fig. 3d of Ref.[27]). The modes at 75.3 meV/75.9 meV and 86.5 meV/86.8 meV are consistent with the 75.0 meV and 85.3 meV observed in recent 2DES experiments[28]. Besides, the modes at about 64.0 meV and 63.4 meV are very close to the mode (65 meV) in the experiments of Davies and Hamer[13]. The JT-active modes obtained from the IDP method are also in good agreement with the results of the AIMD calculations[18]. The small deviation of the frequencies may arise from the fact that the IDP is calculated at 0 K with adiabatic approximation while the AIMD calculations are performed at 10 K or 77 K, which include the nonadiabatic transitions between the excited states  $e_x$  and  $e_y$  orbitals on different APES sheets.

Our calculations suggest that the observed vibrational modes in 2DES measurement have close ties to the JT effect in the excited states of the NV center. Most of them participate in the dynamical process of electron-phonon coupling and play an important role in the JT distortion. Our calculations also conform that the barrier between the minima in the APES is small enough for a thermally activated pseudo-rotation. Specific vibrational modes, like those at 32.1 meV in 2DES[27], are exclusively found in distortion from saddle point to minimum in our calculations. This implies the allowing vibronic

relaxation path (M-S-M-S...) in the APES. Notably, recent AIMD simulations[18] align well with our finding, with vibrational modes obtained from AIMD closely resembling those identified here. This corroborates the reliability and accuracy of the computational methodology employed in the present work. Furthermore, the method we employed can be extended to analyze the multi-mode JT effects in other defect centers, thus facilitating further study of their critical properties such as spin–orbital coupling, dephasing, and relaxation.

**Acknowledgments** Work at Ames Laboratory was supported by the US Department of Energy, Office of Science, Basic Energy Sciences, Division of Materials Science and Engineering, including a grant of computer time at the National

Energy Research Scientific Computing Centre (NERSC) in Berkeley, CA. Ames Laboratory is operated for the U.S. DOE by Iowa State University under contract # DE-AC02-07CH11358. J. H. Zhang was also supported by National Natural Science Foundation of China under Grant Nos.11204257, Natural Science Foundation of Hainan Province (121MS002, 122RC542), and the Research Start-up Fund Project of Hainan University (KYQD(ZR)-21066). Z. Z. Zhu was supported by the National Natural Science Foundation of China under Grant Nos. 21233004. This work is part of the research programme NWO QuTech Physics Funding (QTECH, programme 172) with project number 16QTECH02, which is (partly) financed by the Dutch Research Council (NWO).

- 
- [1] Mete Atatüre, Dirk Englund, Nick Vamivakas, Sang-Yun Lee, and Joerg Wrachtrup. Material platforms for spin-based photonic quantum technologies. *Nature Reviews Materials*, 3(5):38–51, 2018.
  - [2] David D. Awschalom, Ronald Hanson, Jörg Wrachtrup, and Brian B. Zhou. Quantum technologies with optically interfaced solid-state spins. *Nature Photonics*, 12(9):516–527, 2018.
  - [3] L. Rondin, J. P. Tetienne, T. Hingant, J. F. Roch, P. Maletinsky, and V. Jacques. Magnetometry with nitrogen-vacancy defects in diamond. *Reports on Progress in Physics*, 77(5), 2014.
  - [4] Michael Hanks, Michael Trupke, Jorg Schmiedmayer, William J. Munro, and Kae Nemoto. High-fidelity spin measurement on the nitrogen-vacancy center. *New Journal of Physics*, 19, 2017.
  - [5] John F. Barry, Jennifer M. Schloss, Erik Bauch, Matthew J. Turner, Connor A. Hart, Linh M. Pham, and Ronald L. Walsworth. Sensitivity optimization for NV-diamond magnetometry. *Reviews of Modern Physics*, 92(1):015004, 2020.
  - [6] Ziwei Qiu, Uri Vool, Assaf Hamo, and Amir Yacoby. Nuclear spin assisted magnetic field angle sensing. *npj Quantum Information*, 7(1):39, 2021.
  - [7] H. F. Fotsos, A. E. Feiguin, D. D. Awschalom, and V. V. Dobrovitski. Suppressing spectral diffusion of emitted photons with optical pulses. *Physical Review Letters*, 116(3), 2016.
  - [8] Donovan Buterakos, Edwin Barnes, and Sophia E. Economou. Deterministic generation of all-photonic quantum repeaters from solid-state emitters. *Physical Review X*, 7(4), 2017.
  - [9] S. E. Lillie, D. A. Broadway, J. D. A. Wood, D. A. Simpson, A. Stacey, J. P. Tetienne, and L. C. L. Hollenberg. Environmentally mediated coherent control of a spin qubit in diamond. *Physical Review Letters*, 118(16), 2017.
  - [10] M. H. Abobeih, J. Cramer, M. A. Bakker, N. Kalb, M. Markham, D. J. Twitchen, and T. H. Taminiau. One-second coherence for a single electron spin coupled to a multi-qubit nuclear-spin environment. *Nature Communications*, 9, 2018.
  - [11] V. V. Dobrovitski, G. D. Fuchs, A. L. Falk, C. Santori, and D. D. Awschalom. *Quantum Control over Single Spins in Diamond*, volume 4 of *Annual Review of Condensed Matter Physics*, pages 23–50. 2013.
  - [12] Thomas Uden, Nikolas Tomek, Timo Weggler, Florian Frank, Paz London, Jonathan Zopes, Christian Degen, Nicole Raatz, Jan Meijer, Hideyuki Watanabe, Kohei M. Itoh, Martin B. Plenio, Boris Naydenov, and Fedor Jelezko. Coherent control of solid state nuclear spin nano-ensembles. *npj Quantum Information*, 4(1):39, 2018.
  - [13] G. Davies. Vibronic spectra in diamond. *Journal of Physics C: Solid State Physics*, 7(20):3797, 1974.
  - [14] G. D. Fuchs, V. V. Dobrovitski, D. M. Toyli, F. J. Heremans, C. D. Weis, T. Schenkel, and D. D. Awschalom. Excited-state spin coherence of a single nitrogen–vacancy centre in diamond. *Nature Physics*, 6(9):668–672, 2010.
  - [15] S. C. Rand, A. Lenef, and S. W. Brown. Zeeman coherence and quantum beats in ultrafast photon echoes of N-V centers in diamond. *Journal of Luminescence*, 60:739–741, 1994.
  - [16] Kai-Mei C. Fu, Charles Santori, Paul E. Barclay, Lachlan J. Rogers, Neil B. Manson, and Raymond G. Beausoleil. Observation of the dynamic Jahn-Teller effect in the excited states of nitrogen-vacancy centers in diamond. *Physical Review Letters*, 103(25):256404, 2009.
  - [17] Tesfaye A. Abtew, Y. Y. Sun, Bi-Ching Shih, Pratibha Dev, S. B. Zhang, and Peihong Zhang. Dynamic Jahn-Teller effect in the NV<sup>−</sup> center in diamond. *Physical Review Letters*, 107(14):146403, 2011.
  - [18] R. Ulbricht, S. Dong, I. Y. Chang, B. M. K. Mariserla, K. M. Dani, K. Hyeon-Deuk, and Z. H. Loh. Jahn-Teller-induced femtosecond electronic depolarization dynamics of the nitrogen-vacancy defect in diamond. *Nature Communications*, 7:6, 2016.
  - [19] W. L. Ma and S. S. Li. Multiphonon effects on the optical emission spectra of the nitrogen-vacancy center in diamond at different temperatures. *Journal of Applied Physics*, 111(6), 2012.
  - [20] A. Alkauskas, B. B. Buckley, D. D. Awschalom, and C. G. Van de Walle. First-principles theory of the luminescence line-shape for the triplet transition in diamond NV centres. *New Journal of Physics*, 16, 2014.
  - [21] L. Razinkovas, M. W. Doherty, N. B. Manson, C. G. Van de Walle, and A. Alkauskas. Vibrational and vibronic structure of isolated point defects: The nitrogen-vacancy center in diamond. *Physical Review B*, 104(4), 2021.
  - [22] A. Gali, T. Simon, and J. E. Lowther. An ab initio study of local vibration modes of the nitrogen-vacancy center in diamond. *New Journal of Physics*, 13(2):025016, 2011.
  - [23] Jianhua Zhang, Cai-Zhuang Wang, Z. Z. Zhu, and V. V. Dobrovitski. Vibrational modes and lattice distortion of a nitrogen-vacancy center in diamond from first-principles calculations. *Physical Review B*, 84(3):035211, 2011.
  - [24] Gergő Thiering and Adam Gali. Ab initio calculation of spin-orbit coupling for an NV center in diamond exhibiting dynamic Jahn-Teller effect. *Physical Review B*, 96(8):081115, 2017.
  - [25] Isaac B. Bersuker. The Jahn–Teller Effect. *Cambridge University Press, Cambridge, U.K.*, 2006.

- [26] Jianhua Zhang, Cai-Zhuang Wang, Zizhong Zhu, Qing Huo Liu, and Kai-Ming Ho. Multimode Jahn-Teller effect in bulk systems: A case of the  $\text{NV}^0$  center in diamond. *Physical Review B*, 97(16):165204, 2018.
- [27] V. M. Huxter, T. A. A. Oliver, D. Budker, and G. R. Fleming. Vibrational and electronic dynamics of nitrogen-vacancy centres in diamond revealed by two-dimensional ultrafast spectroscopy. *Nature Physics*, 9(11):744–749, 2013.
- [28] William P. Carbery, Camille A. Farfan, Ronald Ulbricht, and Daniel B. Turner. The phonon-modulated Jahn–Teller distortion of the nitrogen vacancy center in diamond. *Nature Communications*, 15(1):8646, 2024.
- [29] N. B. Manson, J. P. Harrison, and M. J. Sellars. Nitrogen-vacancy center in diamond: Model of the electronic structure and associated dynamics. *Physical Review B*, 74(10):104303, 2006.
- [30] G. Kresse and J. Furthmüller. Efficient iterative schemes for ab initio total-energy calculations using a plane-wave basis set. *Physical Review B*, 54(16):11169–11186, 1996.
- [31] Jochen Heyd, Gustavo E. Scuseria, and Matthias Ernzerhof. Hybrid functionals based on a screened coulomb potential. *The Journal of Chemical Physics*, 118(18):8207–8215, 2003.
- [32] C.A. Stüßel C.A. Daul, K. Doclo. *Recent Advances in Density Functional Methods, Part II*, volume 1. WORLD SCIENTIFIC, 1997.
- [33] Matija Zlatar, Carl-Wilhelm Schläpfer, and Claude Daul. *A New Method to Describe the Multimode Jahn–Teller Effect Using Density Functional Theory*, volume 97 of *Springer Series in Chemical Physics*, book section 6, pages 131–165. Springer Berlin Heidelberg, 2009.
- [34] Matija Zlatar, Maja Gruden-Pavlović, Carl-Wilhelm Schläpfer, and Claude Daul. Intrinsic distortion path in the analysis of the Jahn–Teller effect. *Journal of Molecular Structure*, 954(1–3):86–93, 2010.
- [35] Dario Alfè. PHON: A program to calculate phonons using the small displacement method. *Computer Physics Communications*, 180(12):2622–2633, 2009.
- [36] Harry Ramanantoanina, Matija Zlatar, Pablo Garcia-Fernandez, Claude Daul, and Maja Gruden-Pavlovic. General treatment of the multimode Jahn-Teller effect: study of fullerene cations. *Physical Chemistry Chemical Physics*, 15(4):1252–1259, 2013.